RSC Advances

PAPER

View Article Online
View Journal | View Issue

Check for updates

Cite this: *RSC Adv.*, 2019, **9**, 17382

Theoretical study on the electronic structure and second-order nonlinear optical properties of benzannulated or selenophene-annulated expanded helicenes†

Li-jing Gong, ‡*[a] Chun-yu Liu,‡[b] Cheng Ma,[a] Wan-feng Lin,[a] Jin-kai Lv[a] and Xiang-yu Zhang[a]

Received 13th February 2019
Accepted 27th May 2019

DOI: 10.1039/c9ra01136f

rsc.li/rsc-advances

Currently, discovering new materials with superior second-order nonlinear optical (NLO) performance has become a very hot research topic in the fields of chemistry and materials science. Now, density functional theory (DFT) has become a powerful tool to predict the performance of novel materials. In this paper, based on benzannulated and selenophene-annulated expanded helicenes, twenty-six helicenes are designed by introduction donor/acceptor moieties and their combinations at different substituent positions. The geometrical/electronic structures, electronic transition, and second-order NLO properties of these helicenes are full investigated by DFT/TDDFT theory. The investigations show that these helicenes have large first hyperpolarizability values (β_{HRS}). For instance, the β_{HRS} value (29.95×10^{-30} esu) of helicene **H24** is about 7 times larger than that of the highly π-delocalized phenyliminomethyl ferrocene complex. In addition, the introduction of acceptor NO_2 unit at R_7 and R_8 positions for helicenes **H1** and **H15** can obtain the largest β_{HRS} value, which is attributed to the enhancement of electron acceptor ability. In view of large NLO response and intrinsic asymmetric structures, the studied helicenes have the possibility to be excellent second-order NLO materials.

I. Introduction

Helicenes have been defined as polycyclic aromatic hydrocarbons with nonplanar screw-shaped structures formed by *ortho*-fused benzene or other aromatic rings. These helicenes possess many fascinating properties because of their helical molecular geometries, such as large nonlinear optical responses, chiroptical, circular polarized absorption and emission, and relatively high solubility.[1–7] Therefore, they are now sparking extensive attention in the areas of electronics and optoelectronics, nonlinear optics, switches and molecular recognition.[8–14]

In general, the currently studied helicenes can be divided into three types from the perspective of the fused rings arrangement. One type only contains angularly fused rings. The second is the combinations of angular with linear fusion of benzene rings, are viewed as expanded helicenes. The third is laterally π-extended helicenes based on the first type. The latter two types may lead to novel electronic, photophysical and chiroptical properties due to the size increase of a helicene.[15]

A large number of laterally extended helicenes have been well-characterized.[16–19] For example, Collins *et al.* reported that pyrene and [4]- or [5]helicene with an increased π surface displayed significant red-shifts compared to the parent [5]helicene in both the UV/Vis and the fluorescence spectra, and adopts co-planar or stacked arrangements in the solid state.[20] The pyrene-based dibenzo[7]helicene and 2*H*-pyran[7]helicene lateral derivatives with the fluorescent quantum yields in dichloromethane of FF = 0.10 and 0.17 have been reported.[21] They form remarkably stabilised intramolecular excimer states upon excitation and exhibit large Stokes shifts respectively. Nuckolls *et al.*[22] demonstrated that perylenediimide (PDI)-based π-extended helicenes results in the collision of π-electron clouds between two PDI subunits, which enhance the delocalization of electrons. However, the studies of expanded helicenes are very few, especially the study on the modification of their structure.

---

[a] *Aviation University of Air Force, Changchun, 130022 Jilin, China. E-mail: gonglijing@126.com*

[b] *Institute of Functional Material Chemistry, National & Local United Engineering Lab for Power Battery, Faculty of Chemistry, Northeast Normal University, Changchun, 130024 Jilin, China*

† Electronic supplementary information (ESI) available: The selected bond lengths for helicene **H1** between experiment and calculation, the contour plots of the HOMO and LUMO for the studied helicenes **H2–H4**, **H6–H9**, **H11**, **H16–H18** and **H20–H23**, and **H25**, the computed main energy absorption band (λ, nm) at the different basis sets level for helicene **H1**, the computed main energy absorption band (λ, nm) using the different functionals for helicene **H1**, the electron density difference maps of helicenes **H2–H9**, **H11–H14**, **H16–H23** and **H25–H28**, and the calculated β_{HRS} values ($\times 10^{-30}$ esu) of helicenes **H1–H28** by using four DFT functionals are shown. See DOI: 10.1039/c9ra01136f

‡ These authors contributed equally.

Recently, Tilley *et al.*[23] reported a benzannulated or selenophene-annulated expanded helicenes, which is named helicenes **H1** and **H15**, respectively (Fig. 1). They are composed of alternating linearly and angularly fused rings and contain larger π-systems than typical helicenes, and possess an internal cavity. The **H1** forms dimeric structure in the solid state, and no π-stacking interactions between dimers, while helicene **H15** exhibits long-range π-stacking in the solid state. These properties may result in a certain application in the field of organic electronics. Moreover, their unique helical structure arising from the chirality can meet the basic requirement of second-order NLO material. Accordingly, helicenes **H1** and **H15** are likely to be the potential second-order NLO material.

It is well known that macroscopic properties strongly related to microcosmic electron structures, especially for electronic transition properties upon excitation. By all appearances, it is necessary to systemically investigate the photophysical properties and establish structure–property relationships at the quantum chemistry level of theory, so that their performance further improve. To achieve this purpose, twenty-six benzannulated or selenophene-annulated expanded helicenes **H2–H14** and **H16–H28** were designed. The introduction of donor NH_2 unit or acceptor NO_2 unit at R_1 and R_2, or R_3 and R_4, or R_5 and R_6, or R_7 and R_8, or R_9 and R_{10} positions was named as helicenes **H2–H11** and **H16–H25**, respectively. Helicenes **H12**, **H13**, **H26**, **H27** are the simultaneously introduction of donor NH_2 unit or acceptor NO_2 unit at R_1–R_{10} positions. For helicenes **H14** and **H28**, NO_2 unit is at R_1, R_3, R_5, R_7 and R_9 positions, and NH_2 unit is at R_2, R_4, R_6, R_8 and R_{10} positions. In order to more clearly describe the structure and charge transfer properties, we numbered the benzene ring in the helicenes, as shown in Fig. 1. In this paper, our main goal is to shed light with the help of DFT/TDDFT calculations to (i) investigate the frontier molecular orbitals (FMOs) (ii) analyze electronic transition mechanism and (iii) study NLO properties.

II. Computational details

All quantum chemistry calculations were carried out with Gaussian 09 Software.[24] The ground-state geometries of the studied helicenes were optimized using the B3LYP[25] functional. The B3LYP functional is a combination of Becke's three-parameter hybrid exchange functional[26] and the Lee–Yang–Parr[27] correlation functional. Basis sets of the effective core potential (ECP) double-ζ (DZ) LANL2DZ containing relativistic effects for Se and 6-31G(d) for O, N, C and H atoms were

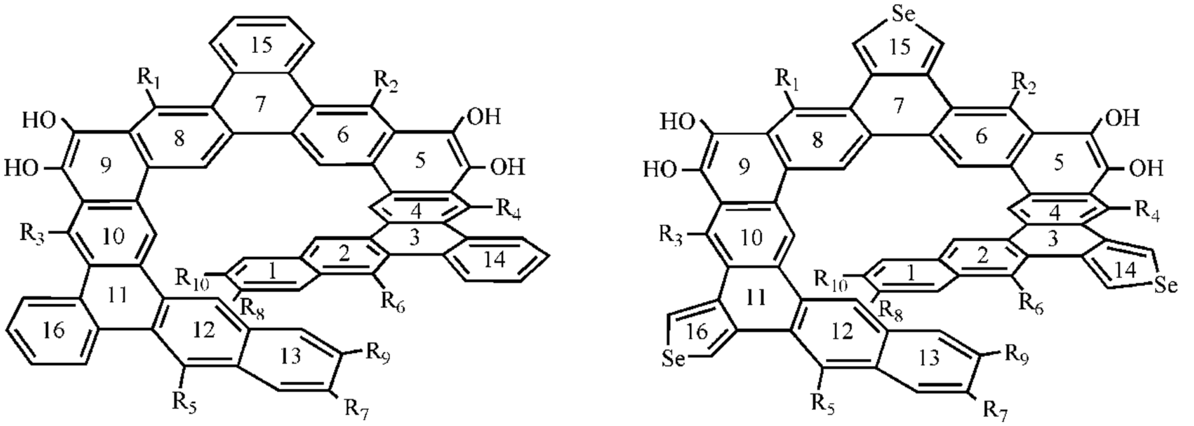

H1: $R_1=R_2=R_3=R_4=R_5=R_6=R_7=R_8=R_9=R_{10}=H$
H2: $R_1=R_2=NH_2$ $R_3=R_4=R_5=R_6=R_7=R_8=R_9=R_{10}=H$
H3: $R_3=R_4=NH_2$ $R_1=R_2=R_5=R_6=R_7=R_8=R_9=R_{10}=H$
H4: $R_5=R_6=NH_2$ $R_1=R_2=R_3=R_4=R_7=R_8=R_9=R_{10}=H$
H5: $R_7=R_8=NH_2$ $R_1=R_2=R_3=R_4=R_5=R_6=R_9=R_{10}=H$
H6: $R_9=R_{10}=NH_2$ $R_1=R_2=R_3=R_4=R_5=R_6=R_7=R_8=H$
H7: $R_1=R_2=NO_2$ $R_3=R_4=R_5=R_6=R_7=R_8=R_9=R_{10}=H$
H8: $R_3=R_4=NO_2$ $R_1=R_2=R_5=R_6=R_7=R_8=R_9=R_{10}=H$
H9: $R_5=R_6=NO_2$ $R_1=R_2=R_3=R_4=R_7=R_8=R_9=R_{10}=H$
H10: $R_7=R_8=NO_2$ $R_1=R_2=R_3=R_4=R_5=R_6=R_9=R_{10}=H$
H11: $R_9=R_{10}=NO_2$ $R_1=R_2=R_3=R_4=R_5=R_6=R_7=R_8=H$
H12: $R_1=R_2=R_3=R_4=R_5=R_6=R_7=R_8=R_9=R_{10}=NH_2$
H13: $R_1=R_2=R_3=R_4=R_5=R_6=R_7=R_8=R_9=R_{10}=NO_2$
H14: $R_1=R_3=R_5=R_7=R_9=NO_2$ $R_2=R_4=R_6=R_8=R_{10}=NH_2$

H15: $R_1=R_2=R_3=R_4=R_5=R_6=R_7=R_8=R_9=R_{10}=H$
H16: $R_1=R_2=NH_2$ $R_3=R_4=R_5=R_6=R_7=R_8=R_9=R_{10}=H$
H17: $R_3=R_4=NH_2$ $R_1=R_2=R_5=R_6=R_7=R_8=R_9=R_{10}=H$
H18: $R_5=R_6=NH_2$ $R_1=R_2=R_3=R_4=R_7=R_8=R_9=R_{10}=H$
H19: $R_7=R_8=NH_2$ $R_1=R_2=R_3=R_4=R_5=R_6=R_9=R_{10}=H$
H20: $R_9=R_{10}=NH_2$ $R_1=R_2=R_3=R_4=R_5=R_6=R_7=R_8=H$
H21: $R_1=R_2=NO_2$ $R_3=R_4=R_5=R_6=R_7=R_8=R_9=R_{10}=H$
H22: $R_3=R_4=NO_2$ $R_1=R_2=R_5=R_6=R_7=R_8=R_9=R_{10}=H$
H23: $R_5=R_6=NO_2$ $R_1=R_2=R_3=R_4=R_7=R_8=R_9=R_{10}=H$
H24: $R_7=R_8=NO_2$ $R_1=R_2=R_3=R_4=R_5=R_6=R_9=R_{10}=H$
H25: $R_9=R_{10}=NO_2$ $R_1=R_2=R_3=R_4=R_5=R_6=R_7=R_8=H$
H26: $R_1=R_2=R_3=R_4=R_5=R_6=R_7=R_8=R_9=R_{10}=NH_2$
H27: $R_1=R_2=R_3=R_4=R_5=R_6=R_7=R_8=R_9=R_{10}=NO_2$
H28: $R_1=R_3=R_5=R_7=R_9=NO_2$ $R_2=R_4=R_6=R_8=R_{10}=NH_2$

Fig. 1 Chemical structures of the studied helicenes H1–H28.

employed. Harmonic vibration frequency calculations were used to ensure the optimized structure is the most stable configuration. During the optimization process, there are no symmetry or internal coordination constraints.

The calculated excitation energies, absorption wavelengths, and oscillator strengths the studied helicenes **H1–H14** were calculated at the TD-B3LYP/6-31+G(d) level and those of the studied helicenes **H15–H28** were calculated at the TD-B3LYP/6-31+G(d)/LANL2DZ level (6-31+G(d) for O, N, C and H atoms; LANL2DZ basis set for Se atom).

It is noted that first hyperpolarizability is an important parameter to evaluate the second-order NLO property. In this paper, the second-order NLO response was determined by hyper-Rayleigh scattering (β_{HRS}), as follows:[28,29]

$$\beta_{\mathrm{HRS}}(0;0,0) = \sqrt{\left\{{\beta_{zzz}}^2 + {\beta_{xzz}}^2\right\}} \tag{1}$$

where, β_{zzz}^2 and β_{xzz}^2 are the orientational average of the first hyperpolarizability tensor without assuming Kleinman's conditions. Only the static first hyperpolarizability was considered.

The associated depolarization ratio (DR), which gives the shape information of the NLO-phore, reads as follows:[30]

$$\mathrm{DR} = \frac{\left\langle {\beta_{zzz}}^2 \right\rangle}{\left\langle {\beta_{\mathrm{ZXX}}}^2 \right\rangle} \tag{2}$$

β is also typically decomposed into the sum of dipolar ($J = 1$) and octupolar ($J = 3$) tensorial components:[31]

$$\left\langle {\beta_{\mathrm{ZZZ}}}^2 \right\rangle = \frac{9}{45}\left|\beta_{J=1}\right|^2 + \frac{6}{105}\left|\beta_{J=3}\right|^3 \tag{3}$$

$$\left\langle {\beta_{\mathrm{ZXX}}}^2 \right\rangle = \frac{1}{45}\left|\beta_{J=1}\right|^2 + \frac{4}{105}\left|\beta_{J=3}\right|^3 \tag{4}$$

The β_{HRS} values ($\times 10^{-30}$ esu) of helicenes **H1–H14** are calculated by using CAM-B3LYP functionals associated with the 6-31+G(d) basis set and the β_{HRS} values ($\times 10^{-30}$ esu) of helicenes **H15–H28** are calculated by using CAM-B3LYP associated with the 6-31+G(d) for O, N, C and H atoms and LANL2DZ basis set for Se atom.

III. Results and discussion

3.1 Molecular structures

In this paper, twenty-eight expanded helicenes were investigated, as shown in Fig. 1. Their ground state geometrical structures have been fully optimized at B3LYP/6-31G(d) or B3LYP/6-31G(d)/LANL2DZ level. The positive vibrational frequencies confirmed that our studied helicenes are dynamically stable. Helicenes **H1** and **H15** has been synthesized and characterized, which possess typical helical structure.[23] It consists of alternating linearly and angularly fused rings, H atom at R_1–R_{10} positions. The X-ray crystal structure unambiguously demonstrated it is helical structures. Taking the helicene **H1** as an example to test the feasibility of the selected functional. Several selected geometric structural parameters are compared with the experimental ones (Table S1†), and it is found that the theoretical values are in good agreement with the experimental ones, indicating that our adopted method is suitable to describe the ground state geometrical structure of the studied helicenes.

3.2 Frontier molecular orbital analysis

For organic helicenes, their frontier molecular orbitals (FMOs) distributions and energy gaps (HOMO–LUMO gap) are closely related to the electronic and optical properties. The sketch of the HOMO and LUMO orbitals, the calculated HOMO/LUMO energy levels, and energy gaps of helicenes **H1–H28** are shown in Fig. 2 and S1.†

For helicene **H1**, its HOMO mainly localizes on rings 4–6, 8–10 and oxygen atoms, and its LUMO mostly localizes on rings 4–13, 15 and 16. For helicenes **H2** and **H3**, their HOMO distributions are almost the same as that of helicene **H1**, but the LUMO of helicene **H2** primary distributes on the inner rings, and that of helicene **H3** largely distributes on rings 6–13, 15 and 16, indicating that the introduction of donor NH_2 unit at R_1 and R_2 or R_3 and R_4 positions has a certain influence on the LUMO distribution of helicene **H1**. For helicenes **H4–H6**, their LUMO distributions are nearly the same as that of helicene **H1**, however, the HOMO distributions of helicenes **H4** and **H5** almost delocalize throughout the inner rings, and that of helicene **H6** mainly localizes on rings 1–6, demonstrating that the introduction of donor NH_2 unit at R_5 and R_6, R_7 and R_8 or R_9 and R_{10} positions in helicene **H1** may change the HOMO distribution. For helicenes **H7–H11**, their HOMO distributions are almost the same as that of helicene **H1**. However, their LUMO distributions are rather sensitive to the position of NO_2 unit. The LUMO distribution of helicene **H7** mainly localizes on rings 8–9 and NO_2 unit attached to ring 8, and that of helicene **H8** localizes on rings 4–5 and NO_2 attached to ring 4, and that of **H9** localizes on rings 1–3 and NO_2 units, while the LUMO distributions of helicenes **H10** and **H11** largely localize on rings 1, 2, 12, 13 and NO_2 units. These signify that acceptor NO_2 unit at different substituent positions may have remarkably influence on LUMO distribution of helicene **H1**. For helicene **H12** with the donor NH_2 unit, its HOMO orbital mainly distributes on rings 5, 6, 8–10 and O atoms, and its LUMO localizes on rings 4–9, 14 and 15, which indicating that the distributions of HOMO and LUMO partially overlap. The HOMO of helicene **H13** locates on rings 4–6, 8–10 and O atoms attached to rings 5 and 9, while the LUMO distributes on the whole molecule. Compared with helicene **H12**, the HOMO and LUMO orbitals distributions of helicene **H14** are clearly separated. Its HOMO distribution mainly localizes on rings 1, 2, 4–6, and N and O atoms attached to rings 1–6, and the LUMO distribution mostly localizes on rings 10–13, 16 and NO_2 units attached to rings 12–13. The changes of FMO distributions, indicating that the introduction of the electron-withdraw units (NO_2) facilitates charge separation of frontier molecular orbital, which is beneficial to realize intramolecular charge transfer from HOMO to LUMO.

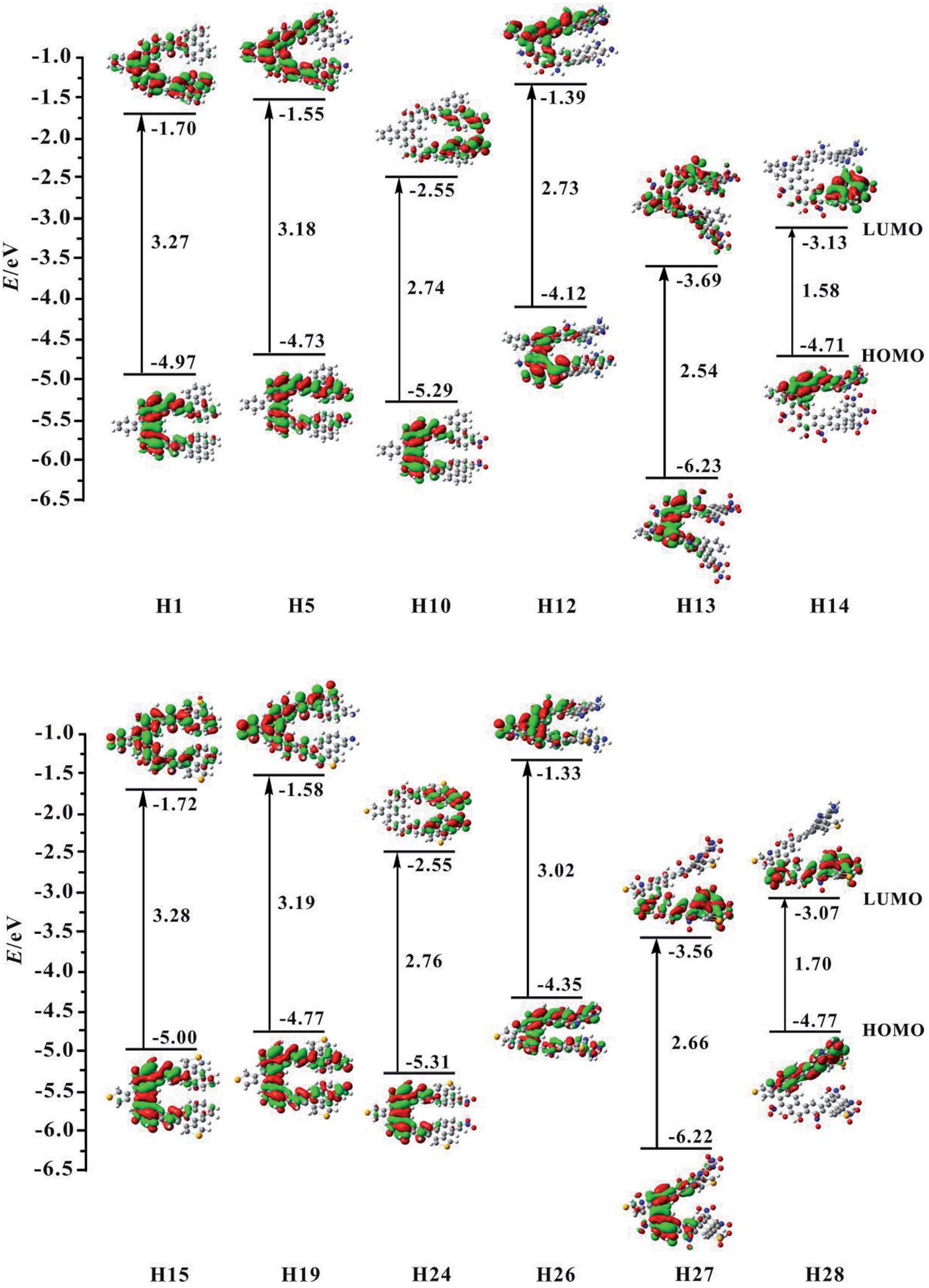

Fig. 2 Contour plots of the HOMO and LUMO for the studied helicenes **H1**, **H5**, **H10**, **H12–H15**, **H19**, **H24**, and **H26–H28**.

For helicene **H15**, its HOMO distribution is almost the same as helicene **H1**. However, its LUMO distribution almost delocalizes over the inner rings and ring 15. For helicene **H16**, its FMOs are nearly the same as that of helicene **H15**. The LUMO distributions of helicenes **H17–H20** are almost the same, distributed on rings 4–10 and 15. However, the HOMO distribution of helicene **H17** is nearly the same as that of helicene **H15**, the HOMOs of helicenes **H18** and **H19** mainly delocalize on inner rings, and the HOMO of helicene **H20** mostly localizes on rings 12, 13, 16 and NH_2 unit attached to ring 13. By observing the FMOs of helicenes **H21–H25**, it can be concluded that the effect of NO_2 unit at different substituent positions on the FMOs of helicene **H15** is almost the same as its effect on the FMOs of helicene **H1**. For helicenes **H26–H28**, their FMOs distributions have significant changes compared with helicene **H15**.

Subsequently, we investigate the effect of the different substituents and substituent positions on energy gap. Compared with helicene **H1**, the HOMO and LUMO energy level of helicenes **H2–H6** slightly increase. However, the increase in HOMO energy levels is greater than the increase in LUMO energy levels, so the bands gap of the five substituted helicenes slightly reduce. It is worth mentioning that the band gap of helicene **H3** is the smallest of the five substituted helicenes, so it can be concluded that the band gap of helicene **H1** can be effectively reduced when the R_3 and R_4 positions are substituted with donor NH_2 unit. For helicenes **H7–H11**, their HOMO and LUMO energy level significantly reduce relative to helicene **H1**. However, the LUMO energy level decreases more rapidly than the HOMO energy level, their band gaps are significantly reduced, which is closely related to the introduction of the NO_2 unit affects the distribution of LUMO in the above analysis. This indicates that the introduction of acceptor NO_2 unit in helicene **H1** can effectively reduce the band gap. In particular, the band gap of helicene **H7** which introduces acceptor NO_2 unit at R_1 and R_2 positions has been reduced to 2.49 eV. For helicene **H12**, its band gap significantly reduces relative to helicenes **H1–H6**, indicating that when the R_1–R_{10} positions are all substituted with donor NH_2 unit, the band gap can be effectively reduced. For helicene **H13**, its band gap also significantly reduced relative to helicene **H1**, but does not much change compared to helicenes **H7–H11**, except that both its HOMO and LUMO energy level greatly reduce. For helicene **H14**, its band gap is the smallest of helicenes **H1–H14**, which results from the electronic distributions of HOMO and LUMO are obviously separated. This indicates that the introduction of the combination of donor NH_2 and acceptor NO_2 unit is an effective method for reducing the band gap of helicene **H1**.

For the homologue **H15** of helicene **H1**, the same substituted way was used in helicene **H15**, which obtained helicenes **H16–H28**. The research found that the HOMO/LUMO energy level and energy gaps of helicenes **H15–H28** have the same conclusions as helicenes **H1–H14**, for example, helicene **H28** which is the introduction of acceptor NO_2 unit at R_1, R_3, R_5, R_7 and R_9 positions and donor NH_2 unit at R_2, R_4, R_6, R_8 and R_{10} positions, has the smallest energy gap in helicenes **H15–H28**. In addition, the electronic structure shows that the visible charge transfer from top (rings 1, 2, 4–6 and N atoms at R_2, R_4, R_6 and R_8 positions) to bottom (rings 8–13 and NO_2 units at R_1, R_5 and R_7 positions) of whole molecule. Overall, FMOs and energy gaps of helicenes **H1** and **H15** can be effectively tuned through introduction of different substituents at proper positions.

3.3 Electronic absorption of helicenes H1–H28

In recent years, the TDDFT method has been widely used in the calculations of electronic transition properties.[32–36] However, proper selection of the functional and basis set is rather important for accurately describing the electronic transition because each functional or basis set has its own merit. Firstly, four Pople's basis sets (*e.g.* 6-31G(d), 6-31G(d,p), 6-31+G(d), and 6-311+G(d)) were selected to evaluate the effect of basis set extension on the electronic absorption wavelength by using B3LYP functional. The calculated main absorption bands of helicene **H1** at the different basis set levels were listed in Table S2.† It is interesting to find that the difference between the absorption wavelengths of the largest basis set and the smallest basis set is about 8 nm. It means that the effect of the basis set size on the calculated absorption wavelength is negligible. Many studies demonstrate that diffuse functions can accurately calculate absorption wavelengths and successfully describe the electronic transition properties.[37,38] Considering the performance and reasonable computational resource, 6-31+G(d) basis set was selected in the following calculation. Subsequently, the B3LYP,[26] M06-2X,[39,40] CAM-B3LYP,[41,42] and BH&HLYP[43] functionals were chosen to test the influence of different functionals on the absorption wavelengths. The results show that the calculated absorption wavelengths of M06-2X, CAM-B3LYP, and BH&HLYP functionals are similar (Table S3†). And, the B3LYP functional slightly underestimates the excitation energy. However, previous studies have shown that the B3LYP functional is the most suitable functional for organic conjugated systems.[44–46] Thus, the B3LYP functional combined with 6-31+G(d) basis set was employed in the following electronic excitation calculations. For the helicenes **H15–H28**, the LANL2DZ basis set was used for Se atom.

Based on the above results of functional or basis set, the 60 lowest electronic excitation energies of the studied helicenes **H1–H14** were calculated at the TD-B3LYP/6-31+G(d) level and those of the studied helicenes **H15–H28** were calculated at the TD-B3LYP/6-31+G(d)/LANL2DZ(6-31+G(d) for O, N, C and H atoms; LANL2DZ basis set for Se atom) level. The calculated excitation energies, absorption wavelengths, and oscillator strengths are summarized in Table 1. To better understand the nature of electronic absorption, electron density difference maps (EDDMs) involved into the most intense band were shown in Fig. 3 and S2.†

Helicene **H1** exhibits one main absorption band with the charge transfer (CT) from rings 4, 5, 12, 13 and 16 to rings 7–11. Helicenes **H2** and **H3** shows three main absorption bands. The most intense absorption band of helicene **H2** is at 313.64 nm, mainly coming from rings 1, 2, 8–10, 12 and 14 to rings 5–7 charge transfer, while that of helicene **H3** mainly originates from the π → π* character on the entire skeleton. For helicene **H4**, there is one main absorption band, the electronic transition is assigned as a CT from rings 2–5, 10, 12, N and O atoms to rings 6–8 and 16. With respect to helicene **H5**, it is interesting to find that there is a CT from rings 11–13 and 16 to the other inner rings, besides π → π* character with rings 7–10. For helicene **H6**, the absorption band locates at 319.90 nm, with the largest oscillator strength, mainly arises from the π → π* character on the entire skeleton. For helicenes **H7** and **H8**, the electronic transition mainly ascribed to the π → π* character on the entire skeleton, while the most intense absorption band

Table 1 Calculated excitation energies (ΔE_{ge}, eV), absorption wavelengths (λ, nm), and oscillator strengths (f) of the studied helicenes **H1**–**H28**

Compound	ΔE_{ge}	λ	f	Compound	ΔE_{ge}	λ	f
H1	3.90	318.21	0.470	**H15**	3.71	334.41	0.911
H2	3.95	313.64	0.301	**H16**	4.12	300.82	0.324
	3.61	343.00	0.216		2.99	414.39	0.172
	2.58	479.76	0.156		2.61	475.71	0.185
H3	4.00	310.00	0.357	**H17**	3.94	314.99	0.161
	3.54	349.96	0.286		3.35	370.15	0.397
	2.54	487.71	0.147		2.81	440.77	0.195
H4	3.88	319.32	0.790	**H18**	3.65	339.48	0.621
H5	3.84	322.64	0.670	**H19**	3.94	314.49	0.430
	3.18	389.41	0.162				
H6	3.88	319.90	0.613	**H20**	3.65	339.52	0.574
	3.28	378.13	0.214				
H7	3.92	316.31	0.606	**H21**	3.66	338.81	0.395
	3.32	373.00	0.102		2.72	465.57	0.135
	2.75	451.32	0.175				
H8	3.87	320.15	0.575	**H22**	3.72	333.53	0.529
	3.53	350.82	0.118				
H9	3.62	342.09	0.326	**H23**	3.72	333.15	0.432
H10	3.68	336.69	0.560	**H24**	3.78	328.22	0.918
	3.17	390.82	0.180		2.67	464.57	0.144
H11	3.75	330.25	0.554	**H25**	3.67	337.52	0.508
H12	3.53	358.80	0.184	**H26**	3.60	344.41	0.199
	2.96	419.10	0.238		3.13	396.23	0.248
	2.50	495.16	0.100				
H13	3.04	407.95	0.124	**H27**	2.99	414.98	0.096
	2.08	596.13	0.121				
H14	2.96	418.79	0.077	**H28**	2.99	414.11	0.093
	2.68	463.13	0.096				

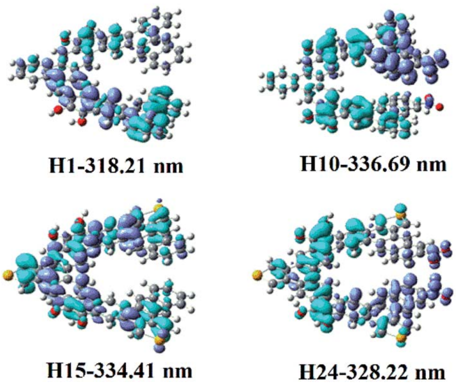

Fig. 3 Electron density difference maps of helicenes **H1**, **H10**, **H15** and **H24**. Blue and purple colours indicate depletion and accumulation of electron density, respectively.

of helicene **H9** originates from rings 1, 2, 12, 13 and 16 to the other rings and NO_2 unit attached to ring 12 charge transfer, and that of helicene **H10** is ascribed to a CT from rings 4, 5, 9, 10, 16 and O atoms attached to rings 5 and 9 to rings 1, 2 and NO_2 attached to ring 1, and that of helicene **H11** comes from rings 12, 13, 16 and C atoms connected to OH units to the other inner rings and NO_2 units CT. For helicene **H12**, it displays three main absorption bands. It is worth mentioning that the oscillator strengths of the second absorption band is largest, this most intense absorption peak at 419.10 nm attributes from rings 5, 6, 9, 10, 12, 13, O atoms and N atoms at R_2, R_3, R_5–R_7 positions to the other rings CT. For helicene **H13**, it has two absorption bands, and its absorption wavelength extended to 596 nm. Its electronic transition arises from rings 8, 10, 15, 16 and C atoms connected to OH units to the NO_2 units at R_1, R_3–R_5, R_7, R_9 and R_{10} positions CT. For helicene **H14**, the oscillator strength of the absorption band is very small, less than 0.1. The most intense absorption band at 463.13 nm has a charge transfer from rings 1, 2, 5, 6, N atoms at R_2, R_4, R_6, R_8, R_{10} positions and O atoms attached to ring 5 to the other inner rings and NO_2 units at R_3, R_5, R_7, R_9 positions, and $\pi \rightarrow \pi^*$ character on rings 4 and 9.

For helicene **H15**, it shows one main absorption band, mainly assigned as $\pi \rightarrow \pi^*$ character on the entire skeleton. The same as helicene **H15**, that of helicene **H19** also ascribed to the $\pi \rightarrow \pi^*$ character on the entire skeleton. Unlike helicene **H15**, that of helicene **H16** comes from rings 12, 13, 15 and 16 to the other rings CT, and that of helicene **H17** originates from rings 1, 2, 11–13, 14 and 16 to the other rings CT, and that of helicene **H18** arises from rings 2, 5–9, 14, O atoms and N atoms to rings 11–13 and 16 CT, and that of helicene **H20** attributes from rings 1, 2 and the N atom at R_{10} position to the other rings CT. For helicene **H21**, the most intense electronic transition is the same as that of helicene **H15**. Unlike helicene **H15**, that of helicene **H22** comes from rings 12, 13, 15 and 16 to NO_2 units CT, and that of helicene **H23** mainly originates from rings 16 to the other rings CT, and that of helicene **H24** arises from rings 4–9 and 14–16 to rings 10–13 and NO_2 units CT, and that of helicene **H25** attributes from rings 14, 15, C atoms connected to OH units to the other rings CT. For helicene **H26**, the second band at 396.23 nm is the most intense absorption, this absorption has a CT and $\pi \rightarrow \pi^*$ character on ring 1–11, 14 and 15. With respect to helicene **H27**, the electronic transition originates from rings 4, 5, 9, 14 and O atoms at rings 5 and 9 to NO_2 units at R_5-R_8 positions CT, besides the $\pi \rightarrow \pi^*$ character within rings 6–8. For helicene **H28**, the electronic transition mainly arises from rings 1, 2, 4, 14 and N atoms attached to rings 1, 2 and 4 to the other rings and NO_2 units attached to ring 13.

Overall, compared with helicene **H1**, the wavelengths of the high-energy absorption band of helicene **H3** are slightly blue-shifted, while those of helicenes **H2**, **H4–H6**, **H7** and **H8** remain essentially unchanged. But those of helicenes **H9–H11** are red-shifted, and those of helicenes **H12–H14** are obviously red shifted ($\Delta\lambda = 40$ nm for helicene **H12**, $\Delta\lambda = 89$ nm for helicene **H13** and $\Delta\lambda = 100$ nm for helicene **H14**). For helicene **H15**, its absorption wavelength is 334.41 nm. Compared with helicene **H15**, the wavelength of the high-energy absorption band of helicenes **H16**, **H17** and **H19** are blue-shifted. The absorption wavelengths of helicenes **H18** and **H20–H25** are close to helicene **H15**. The absorption wavelengths of helicenes **H26–H28** are obviously red-shifted compared with helicene **H15**. In general, the electronic transition properties, absorption wavelength and the number of absorption bands of helicenes **H1** and **H15** can be changed through introduction of different substituents at proper positions.

3.4 Second-order NLO properties

Based on the above analysis, the asymmetric electronic structures of studied helicenes meet the basic requirements for second-order NLO materials. At the same time, the obvious intramolecular CT of these helicenes may result in the large first hyperpolarizability (β_{HRS}). These unique features motivate us to investigate their second-order NLO response.

As we all known, the β_{HRS} is very sensitive to the adopted functionals. Therefore, four popular DFT functionals (*i.e.* B3LYP,[26] CAM-B3LYP,[41,47] M06-2X,[39] and BH&HLYP[48]) were chosen to strengthen the reliability of our calculation results. The calculated β_{HRS} values of helicenes **H1–H28** by four different functionals are given in Table S7.† Among the considered functionals, the β_{HRS} value calculated by B3LYP functional is the largest, whereas the β_{HRS} values obtained by other three functionals are relatively close. Previous studies have shown that the long-range corrected functional CAM-B3LYP is a reliable method to calculate the β_{HRS},[49,50] and B3LYP functional overestimates the β_{HRS}.[51,52] Thus, the β_{HRS} values obtained from CAM-B3LYP were used in the following discussion (Table 2).

The calculated β_{HRS} values of our studied helicenes are large. For example, the β_{HRS} value of the helicene **H24** is (29.95×10^{-30} esu) is about 7 times larger than that of the highly π-delocalized phenyliminomethyl ferrocene complex.[53] Thus, our studied helicenes may be the excellent candidates for second-order NLO materials from the stand point of their large NLO response and intrinsic asymmetric structures. For helicenes **H3**, **H4** and **H6**, their β_{HRS} values are close to the value of helicene **H1**, which indicates that when the R_3 and R_4, R_5 and R_6, or R_9 and R_{10} positions are replaced by donor NH_2 unit, respectively, their effect on the β_{HRS} value is not significant. For helicenes **H2** and **H5**, their β_{HRS} values are about twice that of helicene **H1**, which signifies that the introduction of donor NH_2 unit at R_1 and R_2 or R_7 and R_8 positions can increases the β_{HRS} value. For helicenes **H7–H11**, their β_{HRS} values are larger than helicene **H1**, which shows that the introduction of acceptor NO_2 unit can effective enhance β_{HRS} value. Comparing helicenes **H8–H11** and helicenes **H3–H6**, it is found that the β_{HRS} values of helicene substituted by acceptor NO_2 unit is larger than that of helicene substituted by donor NH_2 unit at the same substituent position, for example, helicene **H8** > helicene **H3**. For helicenes **H12–H14**, their β_{HRS} values are also larger than that of helicene **H1**, which manifests that these three substitution methods are also ways to obtain larger β_{HRS} value. In addition, from helicenes **H1** to **H14**, it can be concluded that the β_{HRS} value of helicene **H10** is the largest of all. This indicates that the maximum β_{HRS} value can be obtained by the introduction of acceptor NO_2 unit at R_7 and R_8 positions for helicene **H1**, which is attributed to the enhancement of electron acceptor ability. For the homolog **H15** of helicene **H1**, the same substituted way was used in helicene **H15**, which obtained helicenes **H16–H28**. It is found that helicenes **H15–H28** have the same conclusions as helicenes **H1–H14**, for example, helicene **H24** which is the introduction of acceptor NO_2 unit at R_7 and R_8 positions, has the largest β_{HRS} value in helicenes **H15–H28**. Comparing helicenes **H15–H28** with **H1–H14**, it can be seen that helicenes **H15–H28** does not have much improvement in NLO response, for example, the β_{HRS} value of helicene **H10** is relatively close to that of helicene **H24**.

Table 2 The calculated β_{HRS} values ($\times 10^{-30}$ esu), depolarization ratios (DRs) and $|\beta_J|$ values ($\times 10^{-30}$ esu) of helicenes **H1–H14** by using CAM-B3LYP functionals associated with the 6-31+G(d) basis set and that of helicenes **H15–H28** by using CAM-B3LYP functionals associated with the 6-31+G(d) for O, N, C and H atoms and LANL2DZ basis set for Se atom

Compound	β_{HRS}	DR	$\lvert\beta_{J=1}\rvert$	$\lvert\beta_{J=3}\rvert$
H1	5.26	3.91	1045.33	1159.44
H2	10.57	6.56	2451.93	1301.30
H3	4.86	2.18	635.11	1541.19
H4	5.02	2.83	838.51	1381.68
H5	9.41	5.68	2111.06	1436.33
H6	5.59	1.71	436.40	1987.46
H7	8.39	4.56	1764.52	1623.98
H8	11.04	6.05	2516.43	1543.56
H9	9.70	5.76	2182.60	1454.95
H10	28.88	6.35	6650.65	3757.64
H11	14.11	5.78	3178.59	2104.02
H12	10.16	3.13	1808.64	2624.92
H13	22.23	6.27	5106.31	2949.23
H14	18.21	5.31	4012.12	3018.81
H15	5.89	3.81	1158.22	1325.11
H16	8.50	4.68	1790.83	1640.37
H17	5.79	2.57	898.50	1682.94
H18	5.72	2.78	945.12	1588.10
H19	10.11	5.69	2268.77	1540.48
H20	5.90	2.63	934.23	1692.44
H21	7.89	3.42	1474.83	1918.88
H22	7.96	4.89	1712.48	1441.10
H23	7.82	4.79	1671.75	1445.51
H24	29.95	6.32	6892.77	3920.86
H25	15.10	5.11	3290.10	2611.43
H26	8.30	2.88	1405.00	2255.36
H27	26.10	5.35	5762.05	4282.72
H28	15.29	5.56	3410.00	2395.30

The depolarization ratio (DR) is also an important parameter of the NLO material, which can be used to reveal the contribution of the β_{HRS} response. Specifically, when the DR is larger than 4.26, the dipolar component makes a major contribution. Reversely, the β_{HRS} response is dominantly from octupolar. For our studied helicenes **H3**, **H4**, **H6**, **H12**, **H17**, **H18**, **H20**, **H21** and **H26**, the octupolar component is dominant. For helicenes **H2**, **H5**, **H8–H11**, **H13**, **H14**, **H19**, **H24**, **H25**, **H27** and **H28** the dipolar part is larger than the octupolar, which becomes more clearly from dipolar ($J = 1$) and octupolar ($J = 3$) tensorial components. However, for helicenes **H1**, **H7**, **H15**, **H16**, **H22** and **H23**, the dipolar part is comparable to the octupolar. Thus, the contribution of dipolar ($J = 1$) and octupolar ($J = 3$) components to the NLO response of helicenes **H1**, **H7**, **H15**, **H16**, **H22** and **H23** are nearly equal.

To better understand their NLO origins, the corresponding electron density difference maps (EDDMs) of helicenes **H1**, **H10**, **H15** and **H24** were shown in Fig. 3. It can be seen that the NLO origin of helicene **H1** attributes to charger transfer (CT) from rings 4, 5, 12, 13 and 16 to rings 7–11, and that of helicene

H15 mainly derives from the localized CT on entire skeleton. Obviously, the CT characters of helicenes **H10** and **H24** are different from helicenes **H1** and **H15**. For instance, the NLO origin of helicene **H10** mainly because of the obvious CT from rings 4, 5, 9, 10, 16 and O attached rings 5 and 9 to rings 1, 2 and NO_2 with ring 1, while that of helicene **H24** originates a CT from rings 4–9 and 14–16 to rings 10–13 and the donor NO_2 parts.

IV. Conclusions

In this paper, we employed DFT/TDDFT theory to investigate photophysical properties of twenty-eight benzannulated or selenophene-annulated expanded helicenes. The investigations show that different substituents at different substituent positions have great effects on electronic structure, electronic absorption and the second-order NLO properties. The introduction of the combination of donor and acceptor units can effectively reduce band gap, and the introduction of donor or acceptor unit at R_1–R_{10} positions enables a large red shift in the absorption wavelength, and the introduction of a NO_2 acceptor unit at R_7 and R_8 positions may obtain the largest first hyperpolarizability values. All these benzannulated or selenophene-annulated expanded helicenes have large first hyperpolarizability values, indicating that the second-order NLO response can be effectively tuned by the introduction of donor or acceptor units or their combination. In view of large NLO response and intrinsic asymmetric structures, these studied helicenes may become the excellent candidates for second-order NLO materials, which will further promote the development of high technological applications.

Conflicts of interest

There are no conflicts to declare.

Acknowledgements

This work is supported by the Education Department of Jilin Province, China, under Grant number 2016511.

Notes and references

1 Y. Shen and C. Chen, *Chem. Rev.*, 2012, **112**, 1463–1535.
2 M. Richard Henri, *Angew. Chem., Int. Ed. Engl.*, 2003, **13**, 649–660.
3 J. Katz Thomas, *Angew. Chem., Int. Ed.*, 2000, **39**, 1921–1923.
4 A. Urbano, *Angew. Chem., Int. Ed.*, 2003, **42**, 3986–3989.
5 M. Daigle, D. Miao, A. Lucotti, M. Tommasini and J. Morin, *Angew. Chem., Int. Ed.*, 2017, **56**, 5946.
6 M. Gingras, *Chem. Soc. Rev.*, 2013, **42**, 968–1006.
7 M. Gingras, *Chem. Soc. Rev.*, 2013, **42**, 1051–1095.
8 T. Fujikawa, Y. Segawa and K. Itami, *J. Am. Chem. Soc.*, 2016, **138**, 3587–3595.
9 T. Wohrle, I. Wurzbach, J. Kirres, A. Kostidou, N. Kapernaum, J. Litterscheidt, J. Haenle, P. Staffeld, A. Baro, F. Giesselmann and S. Laschat, *Chem. Rev.*, 2016, **116**, 1139–1241.
10 R. Pascal, *Chem. Rev.*, 2006, **106**, 4809–4819.
11 S. Choudhary, C. Gozalvez, A. Higelin, I. Krossing, M. Melle-Franco and A. Mateo-Alonso, *Chem.–Eur. J.*, 2014, **20**, 1525–1528.
12 S. More, S. Choudhary, A. Higelin, I. Krossing, M. Melle-Franco and A. Mateo-Alonso, *Chem. Commun.*, 2014, **50**, 1976–1979.
13 D. Cortizo-Lacalle, A. Pertegas, L. Martinez-Sarti, M. Melle-Franco, H. Bolink and A. Mateo-Alonso, *J. Mater. Chem. C*, 2015, **3**, 9170–9174.
14 J. Luo, X. Xu, R. Mao and Q. Miao, *J. Am. Chem. Soc.*, 2012, **134**, 13796–13803.
15 R. Rieger and K. Müllen, *J. Phys. Org. Chem.*, 2010, **23**, 315–325.
16 T. Fujikawa, Y. Segawa and K. Itami, *J. Org. Chem.*, 2017, **82**, 7745–7749.
17 T. Fujikawa, Y. Segawa and K. Itami, *J. Am. Chem. Soc.*, 2016, **138**, 3587–3595.
18 Y. Zhu, Z. Xia, Z. Cai, Z. Yuan, N. Jiang, T. Li, Y. Wang, X. Guo, Z. Li, S. Ma, D. Zhong, Y. Li and J. Wang, *J. Am. Chem. Soc.*, 2018, **140**, 4222–4226.
19 T. Hosokawa, Y. Takahashi, T. Matsushima, S. Watanabe, S. Kikkawa, I. Azumaya, A. Tsurusaki and K. Kamikawa, *J. Am. Chem. Soc.*, 2017, **139**, 18512–18521.
20 A. Bédard, A. Vlassova, A. C. Hernandez-Perez, A. Bessette, G. S. Hanan, M. A. Heuft and S. K. Collins, *Chem.–Eur. J.*, 2013, **19**, 16295–16302.
21 M. Buchta, J. Rybáček, A. Jančařík, A. A. Kudale, M. Buděšínský, J. V. Chocholoušová, J. Vacek, L. Bednárová, I. Císařová and G. J. Bodwell, *Chem.–Eur. J.*, 2015, **21**, 8910–8917.
22 N. J. Schuster, D. W. Paley, S. Jockusch, F. Ng, M. L. Steigerwald and C. Nuckolls, *Angew. Chem., Int. Ed.*, 2016, **55**, 13519–13523.
23 G. R. Kiel, S. C. Patel, P. W. Smith, D. S. Levine and T. D. Tilley, *J. Am. Chem. Soc.*, 2017, **139**, 18456–18459.
24 M. W. Evans and G. Wagnière, *Phys. Rev. A*, 1990, **42**, 6732–6736.
25 A. D. Becke, *Phys. Rev. A*, 1988, **38**, 3098–3100.
26 A. D. Becke, *J. Chem. Phys.*, 1993, **98**, 5648–5652.
27 C. Lee, W. Yang and R. G. Parr, *Phys. Rev. B: Condens. Matter Mater. Phys.*, 1988, **37**, 785–789.
28 F. Mançois, L. Sanguinet, J.-L. Pozzo, M. Guillaume, B. Champagne, V. Rodriguez, F. Adamietz, L. Ducasse and F. Castet, *J. Phys. Chem. B*, 2007, **111**, 9795–9802.
29 A. Plaquet, M. Guillaume, B. Champagne, F. Castet, L. Ducasse, J.-L. Pozzo and V. Rodriguez, *Phys. Chem. Chem. Phys.*, 2008, **10**, 6223–6232.
30 M. de Wergifosse, J. de Ruyck and B. Champagne, *J. Phys. Chem. C*, 2014, **118**, 8595–8602.
31 P. Beaujean, F. Bondu, A. Plaquet, J. Garcia-Amorós, J. Cusido, F. M. Raymo, F. Castet, V. Rodriguez and B. Champagne, *J. Am. Chem. Soc.*, 2016, **138**, 5052–5062.
32 G. Scalmani, M. J. Frisch, B. Mennucci, J. Tomasi, R. Cammi and V. Barone, *J. Chem. Phys.*, 2006, **124**, 094107.
33 F. Furche and R. Ahlrichs, *J. Chem. Phys.*, 2004, **121**, 12772–12773.

34 C. Liu, Y. Si, S. Shi, G. Yang and X. Pan, *Dalton Trans.*, 2016, **45**, 7285–7293.

35 D. Jacquemin, B. Mennucci and C. Adamo, *Phys. Chem. Chem. Phys.*, 2011, **13**, 16987–16998.

36 C. Guido, D. Jacquemin, C. Adamo and B. Mennucci, *J. Chem. Theory Comput.*, 2015, **11**, 5782–5790.

37 S. Grimme, *J. Comput. Chem.*, 2004, **25**, 1463–1473.

38 L. Wang, W.-Y. Wang, Y.-Q. Qiu and H.-Z. Lu, *J. Phys. Chem. C*, 2015, **119**, 24965–24975.

39 J.-L. Chen, J.-T. Hong, K.-J. Wu and W.-P. Hu, *Chem. Phys. Lett.*, 2009, **468**, 307–312.

40 E. G. Hohenstein, S. T. Chill and C. D. Sherrill, *J. Chem. Theory Comput.*, 2008, **4**, 1996–2000.

41 A. Pedone, *J. Chem. Theory Comput.*, 2013, **9**, 4087–4096.

42 A. B. Tathe, L. Rhyman, P. Ramasami and N. Sekar, *J. Fluoresc.*, 2015, **25**, 1117–1126.

43 A. Sorkin, M. A. Iron and D. G. Truhlar, *J. Chem. Theory Comput.*, 2008, **4**, 307–315.

44 L. Y. Zou, A. M. Ren, J. K. Feng, Y. L. Liu, X. Q. Ran and C. C. Sun, *J. Phys. Chem. A*, 2008, **112**, 12172–12178.

45 Y. He, Y. Huang, J. Li, X. Pang and G. Yang, *Org. Electron.*, 2017, **50**, 220–227.

46 C. Liu, Y. Si, X. Pan and G. Yang, *RSC Adv.*, 2015, **5**, 72907–72915.

47 T. Yanai, D. P. Tew and N. C. Handy, *Chem. Phys. Lett.*, 2004, **393**, 51–57.

48 I. H. Nayyar, A. E. Masunov and S. Tretiak, *J. Phys. Chem. C*, 2013, **117**, 18170–18189.

49 M. Torrent-Sucarrat, J. Anglada and J. Luis, *J. Chem. Theory Comput.*, 2011, **7**, 3935–3943.

50 M. de Wergifosse and B. Champagne, *J. Chem. Phys.*, 2011, **134**, 074113.

51 H. Sun and J. Autschbach, *ChemPhysChem*, 2013, **14**, 2450–2461.

52 S. J. A. Van Gisbergen, J. G. Snijders and E. J. Baerends, *J. Chem. Phys.*, 1998, **109**, 10657–10668.

53 S. K. Pal, A. Krishnan, P. K. Das and A. G. Samuelson, *J. Organomet. Chem.*, 2000, **604**, 248–259.